Iranian Journal of Astronomy and Astrophysics
Vol. 11, No. 3, Summer 2024, 213–229
©Available online at http://ijaa.du.ac.ir
DOI: 10.22128/ijaa.2025.912.1198
Online ISSN: 2383–403X

Iranian Journal of Astronomy and Astrophysics

Research Paper

Investigating the Sensitivity of Alfvén Pulse Interactions to Plasma Beta in the Corona

Naser Karimi*[1] · Mahdi Alizadeh[2] · Zianab Shajei[3]

[1] Department of Physics Education, Frahangian University, P.O.Box 14665–889, Tehran, Iran;
*email: n.karimi@cfu.ac.ir

[2] Independant researcher, Tabriz, Iran;
email: mah.alizadeh1997@gmail.com

[3] Department of Physics Education, Frahangian University, P.O.Box 14665–889, Tehran, Iran;
email: zshaji1107@gmail.com

Received: 26 November 2024; **Accepted:** 2 January 2025; **Published:** 4 January 2025

Abstract. Two competing theories, the wave theory and reconnection theory, provide explanations for solar corona heating, supported by observations of wave phenomena and magnetic reconnection on the Sun. Plasma β, the ratio of thermal plasma pressure to magnetic pressure, varies significantly in the solar corona, influencing wave propagation Throughout much of the corona, the plasma β is considerably smaller than one, to disregard pressure gradients in the plasma. However, plasma β fluctuates throughout the entire region due to the varying magnetic field, such that near null points, the magnetic field diminishes, leading to a potential increase in plasma β. This study focuses on Alfvén pulses interacting with a 2D magnetic null point, investigating the nonlinear effects of plasma beta adjustment in different layers. The study utilizes the PLUTO code, a sophisticated shock-capturing numerical framework, to model the interactions of Alfvén pulses under varying plasma β conditions. The simulations are conducted on high-resolution Cartesian grids with zero-gradient boundary conditions to ensure accuracy. By solving the magnetohydrodynamic (MHD) equations, the analysis reveals temporal fluctuations in the system's response, with certain instances characterized by higher amplitudes and sharper peaks, indicative of intensified interactions of the Alfvén pulse. The variations in amplitude and peak sharpness underscore the dynamic nature of the system, with certain moments displaying stronger responses than others. On the one hand, when we adjust the plasma beta closer to the null point, the changes in radial velocity and density disturbance decrease, and over time, the wave energy is released more rapidly along the field lines. Density and velocity changes depend on plasma β and proximity to the null point, emphasizing the system's sensitivity to these parameters. Therefore, it is essential to consider atmospheric conditions for accurate energy transfer assessments.

Keywords: Sun, Magnetohydrodynamics, Alfven pulses, Magnetic Null Point, Plasma beta

1 Introduction

MHD waves are crucial for understanding various astrophysical phenomena, including solar flares, coronal heating, and the dynamics of the solar wind. This fascinating topic have

* *Corresponding author*

become a prevalent phenomenon in the Sun's atmosphere [1]. Research into MHD waves for understanding solar plasma structures began in the late 1970s [2,3]. However, it wasn't until the late 1990s that the first observations of kink oscillations, both spatially and temporally resolved, were reported. [4,5], significantly enhancing the effectiveness of theoretical MHD wave models in coronal seismology [6–10]. The process of coronal heating is a complex and crucial aspect of the solar atmosphere. Understanding the mechanisms behind plasma heating is a challenging endeavor. While certain features of the solar atmosphere seem independent, others are interconnected in a chain reaction. For instance, the formation of a magnetic quadrupole, established by the presence of two loops, leads to the development of a current sheet between the smaller loop and the larger loop. This current sheet becomes unstable due to the evolution of the smaller loop, resulting in the formation of a reconnection site where outflows are ejected [11,12]. These outflows, known as type I or II spicules or jets [13], vary in size depending on their origin.

The behavior of MHD waves is significantly influenced by the underlying magnetic structure or topology. Therefore, comprehending the physics of these phenomena necessitates a thorough examination of the topology [14–16] and the behavior of magnetic fields, especially the significance of magnetic null points [17–20], which are prominent in reconnection sites. In the context of this study, the results and conclusions are derived from MHD theory. In addition to examining Alfven waves in solar jets and loops [21], attention must also be directed toward Alfven waves approaching magnetic null points. This interaction induces both fast and slow magnetoacoustic waves [22,23], coupled with compressive waves [24], all contributing to coronal heating through dissipation processes [25].

Building upon the historical understanding of MHD waves, this study examines the nonlinear effects of Alfvén pulses near null points. Before exploring the theory and model, it is crucial to offer a brief historical overview of magnetic null points in the solar corona [26]. A null point in a magnetic field configuration is a point where the magnetic field strength is zero. This can occur in complex magnetic field structures, such as those found in the solar atmosphere or in laboratory plasmas. Near a null point, the magnetic field lines converge towards the null point and can change their topology. The behavior of MHD waves is significantly influenced by the magnetic field configuration around these points. The importance of studying magnetic null points became evident with the discovery of their oscillatory behavior [27] and evolution, particularly through two-dimensional studies. These studies adhered to the initial model created to characterize waves around two-dimensional magnetic null points, uncovering differences in the behavior of Alfven waves and magnetoacoustic waves [28]. This observation laid the foundation for understanding the separate propagation of various modes [28]. Depending on the polarization of the Alfven wave, its effects can differ. A comparison of the non-linear forces related to the plane Alfven wave and the torsional Alfven wave [29,30] has been conducted by Vasheghani Farahani et al. [31], where, for example, it was demonstrated that for plane Alfven waves [32–34] the shock formation time is proportional to the plasma-β, while the shock formation time for torsional Alfven [35] waves is independent of the plasma-β. A wave that does not disturb the adjacent magnetic field lines accumulates along the separatrices without crossing them. Meanwhile, the compressive modes refract along the Alfven-speed profile and gather at the null point [36]. Since the initial pulse is incompressible in the context of the present study, the way compressible waves are generated [37] and organized [38] by the incompressible pulse is emphasized. Before this study, the excitation of transverse and longitudinal waves caused by the plane Alfven wave near a magnetic null point had been examined [39] . They indicate that the formation of these daughter waves is a non-linear effect related to the ponderomotive force. This study aims to analyze nonlinear Alfvén wave behavior near magnetic null points under varying plasma β conditions, a key factor in coronal heating processes. In fact, the objective of

this study is to investigate the behavior of nonlinear fast Alfven waves near a 2D magnetic null point within a finite plasma β regime across different layers. Specifically, we analyze the influence of plasma β on various layers by examining variations in plasma density and radial velocity. To achieve this, numerical simulations are conducted using the PLUTO code [40,41], a finite-volume, shock-capturing code that operates on double precision arithmetic [42]. The subsequent section outlines the fundamental equations and initial setup, while section 2 focuses on model and analytical framework, and section 3 examines the simulation of the magnetoacoustic wave approaching a magnetic null point. Section 4 presents the results and discussion. Finally, section 5 offers a concise conclusion and outlook for future research.

2 Model and Analytical Framework

The modeling and analytical framework of MHD waves involve a combination of fluid dynamics and electromagnetic theory. This framework allows us to analyze the behavior of conducting fluids in the presence of magnetic fields. In the context of this study, our numerical results are based on MHD theory. MHD waves are oscillations that occur in a magnetized plasma, where the dynamics of the fluid and the influences of electromagnetic fields are coupled. These waves arise from the interaction between the motion of the plasma and the magnetic field, making them essential for understanding various physical processes in astrophysical environments, like solar flares and the solar wind, as well as in laboratory plasmas. In the context of this study, our numerical results are based on MHD theory. Building upon the work of Gruszecki et al. [25,27], our model takes into account finite plasma-β conditions. It is important to highlight the well-known resistive MHD equations in the absence of gravity, which are as follows

$$\frac{\partial \rho}{\partial \mathrm{t}} + \nabla . (\rho \mathbf{v}) = 0, \tag{1}$$

$$\rho \left[\frac{\partial \mathbf{v}}{\partial \mathrm{t}} + \rho (\mathbf{v} . \nabla) \mathbf{v} \right] = -\nabla \mathrm{P} + \frac{1}{\mu} (\nabla \times \mathbf{B}) \times \mathbf{B}, \tag{2}$$

$$\rho \left[\frac{\partial \epsilon}{\partial \mathrm{t}} + (\mathbf{v} . \nabla) \epsilon \right] = -\mathrm{P} \nabla . \mathbf{v} + \frac{1}{\sigma} |\mathbf{J}|^2 + \Lambda, \tag{3}$$

$$\frac{\partial \mathbf{B}}{\partial \mathrm{t}} = \nabla \times (\mathbf{v} \times \mathbf{B}) + \eta \nabla^2 \mathbf{B}. \tag{4}$$

It is essential to emphasize that the magnetic field B meets the condition ∇ . B = 0, and the electric current density J is given by $\mathbf{J} = \nabla \times \mathbf{B}/\mu$. Additionally, the physical variables ρ, p, and v represent the density, plasma pressure, and velocity, respectively. Here, $\mu = 4\pi \times 10^{-7}$ H m^{-1}represents the magnetic permeability, σ stands for the electrical conductivity, which is inversely proportional to the magnetic diffusivity η. The internal energy density ϵ is defined as $P/[\rho(\gamma - 1)]$, where γ, the ratio of specific heats, is set to 5/3, as discussed in Karampelas et al. [42].

We analyze a static and homogeneous medium characterized by constant density and pressure (ρ_0, p_0), enveloped within a uniform magnetic field. This assumption simplifies the model but limits its applicability to highly dynamic regions. Our approach involves linearizing the MHD equations, presuming a small disturbance. Beginning with the standard MHD equations (equations 1 to 4), which describe the dynamics of a fully ionized plasma akin to a perfect gas, we apply the continuity equation. Assuming $\Lambda = \eta = 0$ and denoting equilibrium quantities with subscript 0 and perturbed quantities with subscript 1, the linearized

equation of motion can be written as

$$\frac{\partial \rho_1}{\partial t} + \rho_0 \boldsymbol{\nabla}.\boldsymbol{v_1} = 0, \tag{5}$$

$$\rho_0 \frac{\partial \boldsymbol{v_1}}{\partial t} + \boldsymbol{\nabla} p_1 = (\ \boldsymbol{\nabla} \times \boldsymbol{B_1}) \times \boldsymbol{B_0}, \tag{6}$$

$$\frac{\partial \mathbf{B_1}}{\partial t} - \boldsymbol{\nabla} \times (\boldsymbol{v_1} \times \boldsymbol{B_0}) = 0, \tag{7}$$

$$\frac{\partial p_1}{\partial t} + \gamma p_0 \boldsymbol{\nabla}.\boldsymbol{v_1} = 0. \tag{8}$$

The initial magnetic field is characterized as $\mathbf{B} = \mathbf{B}_0$[x/L, −y/L, 0], where B_0 represents the magnetic field strength and L denotes a characteristic length scale. Figure 1 shows the snapshots of the equilibrium magnetic field strength at $t = 0$. Throughout much of the corona, the plasma β is significantly smaller than one, enabling us to overlook pressure gradients in the plasma. However, near null points, the magnetic field weakens, resulting in a possible increase in plasma β.

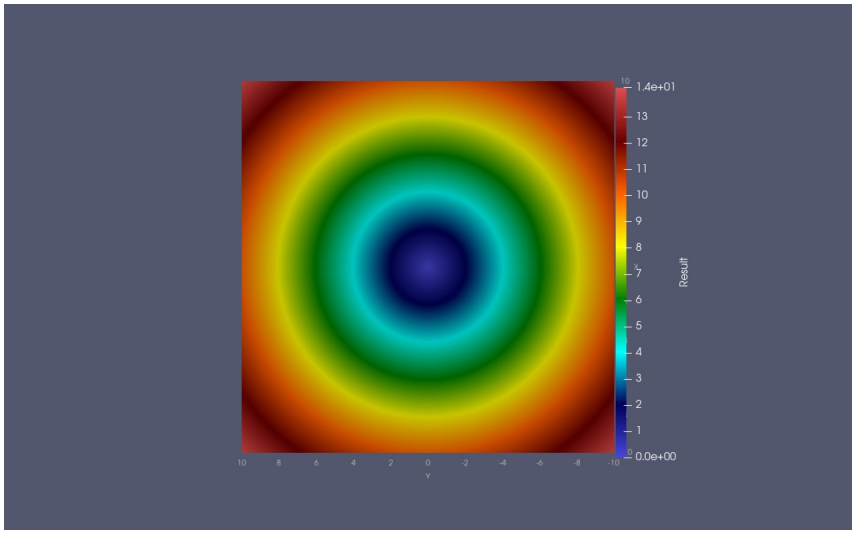

Figure 1: Snapshots of the equilibrium magnetic strength at $t = 0$.

Therefore, understanding the changes in plasma β is essential in this context. Considering equilibrium quantities 18.

$$\beta = \frac{2\mu \mathrm{p_0}}{\mathrm{B}^2} \quad \Longrightarrow \quad \beta = \frac{\beta_0}{\mathrm{x}^2 + y^2} = \frac{\beta_0}{\mathrm{r}^2},$$

where

$$r^2 = \ x^2 + y^2, \ \ \beta_0 = \frac{2\mu p_0 L^2}{B_0^2}.$$

Therefore, plasma β varies across the entire region due to the changing magnetic field throughout our model. Notably, plasma β becomes infinite at the null point. Specifically, beyond a radius of unity, we find a low β environment, while within it, a high β environment prevails. This discrepancy has significant implications, as fast and slow waves display distinct properties depending on their surroundings. Alfvén waves are transverse

waves that propagate along magnetic field lines. They are characterized by oscillations of the plasma with respect to the magnetic field. Alfvén waves play a crucial role in space physics, particularly in the solar wind and magnetosphere. To investigate the behavior of Alfvén waves near a 2D null point, we begin by perturbing our system from its equilibrium state. For this purpose, we introduce a circular initial Alfven pulse centered at the origin, with a circumference of 2πr1, as described by the following equation [43,44]

$$V_z = A_0 \sin\left(\pi \frac{\sqrt{x^2+y^2}-r_1}{r_0}\right) \frac{B_y}{{B_x}^2+{B_y}^2}.$$

In the vicinity of a magnetic null point, we define, $r_1 < \sqrt{x^2+y^2} < r_1 + r_0$, where $V_x = V_y = 0$ and A_0=1 is set as the initial amplitude of the circular as the initial amplitude of thecircular Alfven pulse.

3 Numerical Setup

The framework of this study builds upon earlier research by Karampelas et al. [42], concentrating on plasma density spikes caused by fluctuations in atmospheric conditions, especially plasma-β. Utilizing the PLUTO code, which is well-suited for MHD-based models, we implement a finite-volume shock-capturing approach. In Cartesian coordinates, our numerical procedure determines the time step using the third-order Runge-Kutta method. Spatial integration utilizes the fifth-order monotonicity-preserving scheme (MP5) along with the total variation diminishing Lax-Friedrich solver (TVDLF). Notably, the code variable U_c is normalized by U_0 to account fo various solar atmospheric and plasma-β conditions. The simulation domain spans (-10, 10) × (-10, 10) Mm with a grid resolution of 2500 × 2500 points. Note that we are using zero-gradient boundary conditions here. The PLUTO code functions with dimensionless quantities, necessitating the definition of three essential parameters: ρ_0 , L_0 and v_0, to ensure consistency across all physical quantities. Typically, we set $L_0 = 10^6$ m as the unit length, $\rho_0 = 10^{-12}\frac{Kg}{m^3}$as the unit density, and $B_0 = 10^{-3}\,(T)$ as the unit magnetic field. Additionally, we establish $r_1 = 5$ Mm and $r_0 = 1$ Mm. We $v_0 = \frac{B_0}{\sqrt{\mu\rho_0}}$ to maintain v_0 as a constant background Alfvén speed.

In this study, we investigate nonlinear Alfvén waves with$A_0 = 1$ for layers $r = 1, r = \frac{1}{\sqrt{10}}$ and $r = \frac{1}{10}$, focusing on the perturbation of plasma density and radial velocity induced by the propagation of Alfven waves. We begin by introducing a symmetric Alfven wave to explore the nonlinear dynamics that arise from the interaction of these waves with magnetic null points within the framework of MHD waves and coronal heating.

4 Results and discussion

As MHD waves propagate, the plasma density, pressure, and temperature fluctuate. According to the equation $\beta = \frac{\beta_0}{r^2}$, if β_0 is considered to be zero, then β will also be zero for various values of r. Conversely, if β_0 is taken to be one, β will vary for different values of r.

Figures 2 to 5 illustrate the radial velocity of the Alfven pulse as it approaches the magnetic null point under two atmospheric conditions, represented by β_0=0, β_0=1, for layers $r = 1$, $r = 0.32$, and $r = 0.1$, across seven snapshots at various time instances $t = 0s$, $t = 0.4s$, $t = 1s$, $t = 2s$, and $t = 4s$. These figures illustrate the dynamic behavior of the Alfven pulse over time, emphasizing how the radial velocity of the pulse varies with the plasma β value and the distance of the layers from the null point as the wave propagates

through the medium. Initially, the pulse divides into two waves because of spatial variations in phase speed. The pulse shape changes from circular to elliptical-like due to the azimuthal angle dependence of the nonlinear coefficient. For additional clarity, Figure 14 illustrates the absolute values of the radial velocity along the line $y = x$.

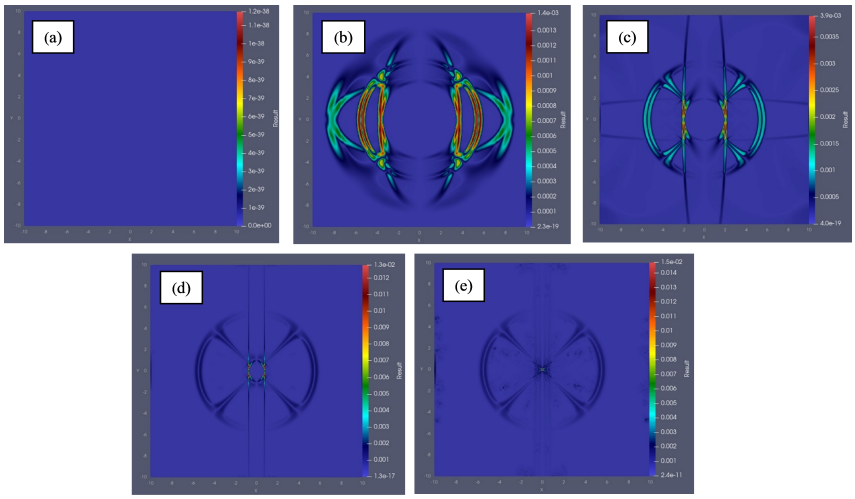

Figure 2: Snapshots of the radial velocity in the inwardly at (a) $t = 0$, (b) $t = 0.4$, (c) $t = 1$, (d) $t = 2$, (e) $t = 4$, propagating pulse of rarefaction, $v_r = \sqrt{v_x^2 + v_y^2}$ as a function of the radial coordinate r for $\beta_0 = 0$.

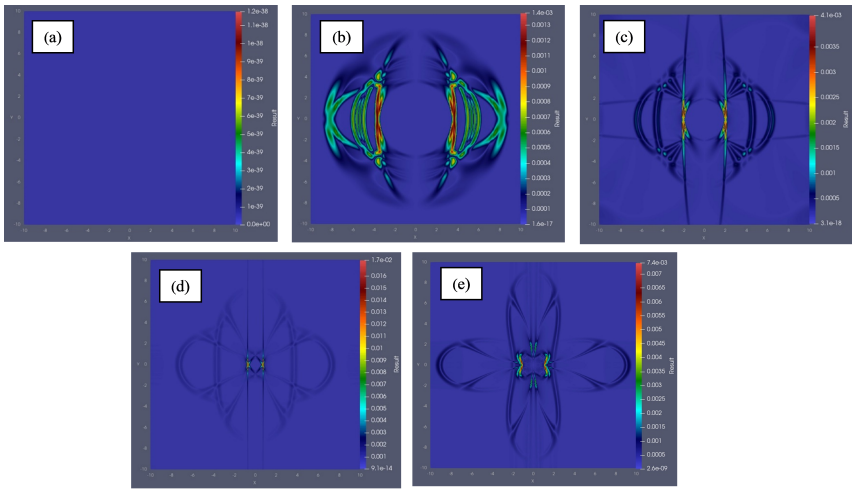

Figure 3: Snapshots of the radial velocity in the inwardly propagating pulse of rarefaction, $v_r = \sqrt{v_x^2 + v_y^2}$ as a function of the radial coordinate r for β_0=1 and r=1 at (a) $t = 0$, (b) $t = 0.4$, (c) $t = 1$, (d) $t = 2$, (e) $t = 4$.

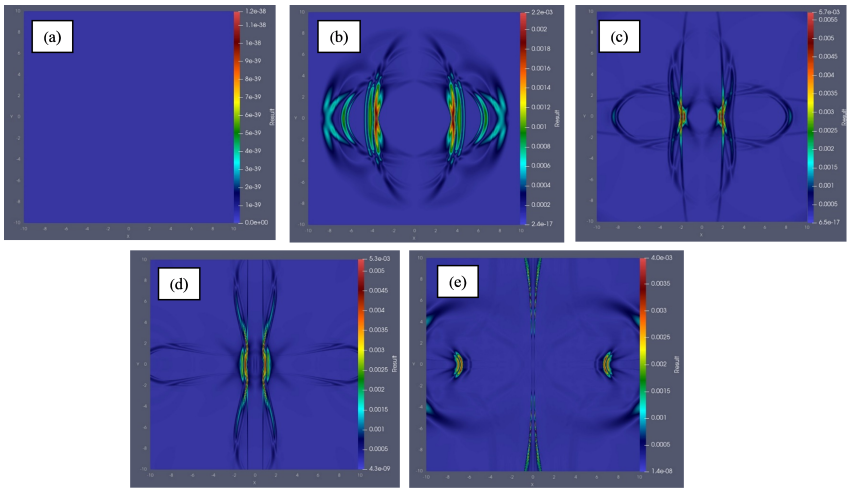

Figure 4: Snapshots of the radial velocity in the inwardly propagating pulse of rarefaction, $v_r = \sqrt{v_x^2 + v_y^2}$ as a function of the radial coordinate r for β_0=1 and r = $\frac{1}{\sqrt{10}}$ at (a) $t = 0$, (b) $t = 0.4$, (c) $t = 1$, (d) $t = 2$, (e) $t = 4$.

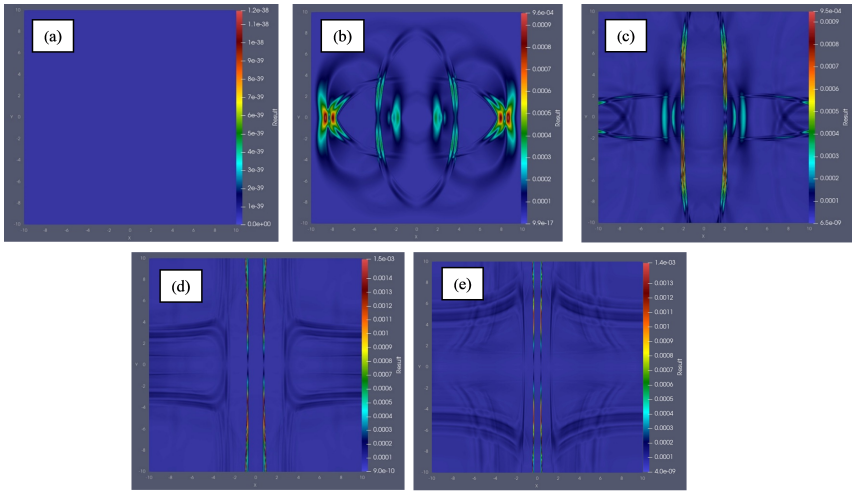

Figure 5: Snapshots of the radial velocity in the inwardly propagating pulse of rarefaction, $v_r = \sqrt{v_x^2 + v_y^2}$ as a function of the radial coordinate r for β_0=1 and r= $\frac{1}{10}$ at (a) $t = 0$, (b) $t = 0.4$, (c) $t = 1$, (d) $t = 2$, (e) $t = 4$.

Figures 6 to 9 illustrate snapshots of the z velocity (v_z) propagating pulse for $t = 0$, $t = 0.4$, $t = 1$, $t = 2$, and $t = 4$ of the Alfvén wave, where the initial pulse has been intrinsically divided into two propagating waves. It is evident that, due to the nature of Alfvén waves, the circular shape of the pulse deforms to align with the magnetic field lines. The Alfvén pulse propagates along the separatrices and accumulates along them. As the

null point is magnetic free, the Alfvén speed drops to zero at that specific point, preventing the presence of Alfvén waves at the null point.

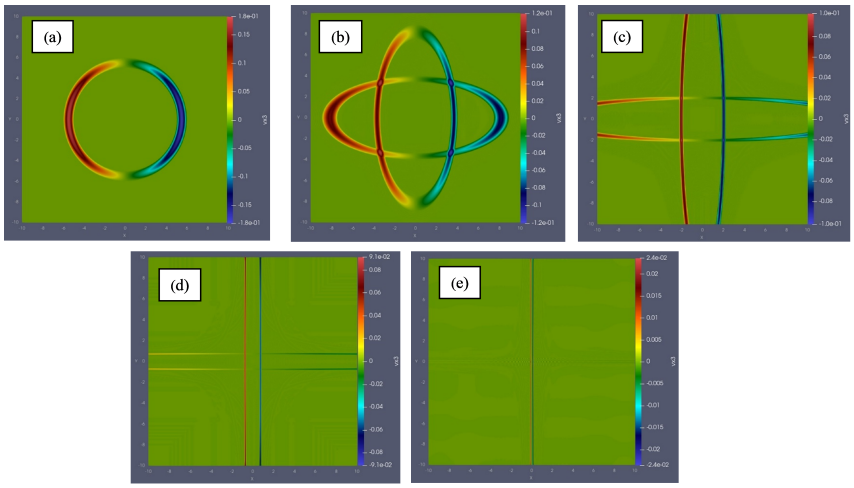

Figure 6: Snapshots of the z velocity (v_z) in the inwardly propagating pulse of rarefaction, for β_0=0 at (a) $t = 0$, (b) $t = 0.4$, (c) $t = 1$, (d) $t = 2$, (e) $t = 4$.

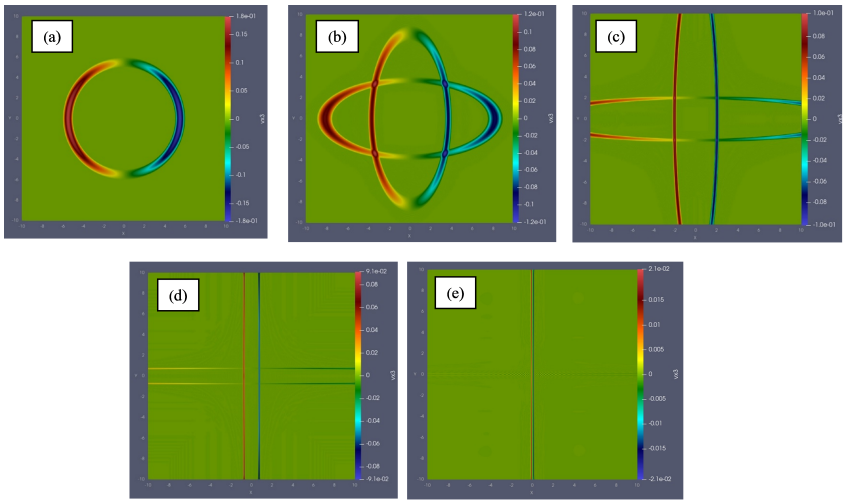

Figure 7: Snapshots of the z velocity (v_z) in the inwardly propagating pulse of rarefaction, for β_0=1 and r=1 at (a) $t = 0$, (b) $t = 0.4$, (c) $t = 1$, (d) $t = 2$, (e) $t = 4$.

To draw a conclusive result, it is essential to observe the variations in mass density resulting from different plasma-β conditions. The dependency of mass density on plasma-β is clearly illustrated in the three snapshots from Figures 10 to 13. This dependency is further emphasized in Figure 15 along the line $y = x$, highlighting the significance of plasma β in influencing density variations. As previously mentioned, the pulse shape transitions

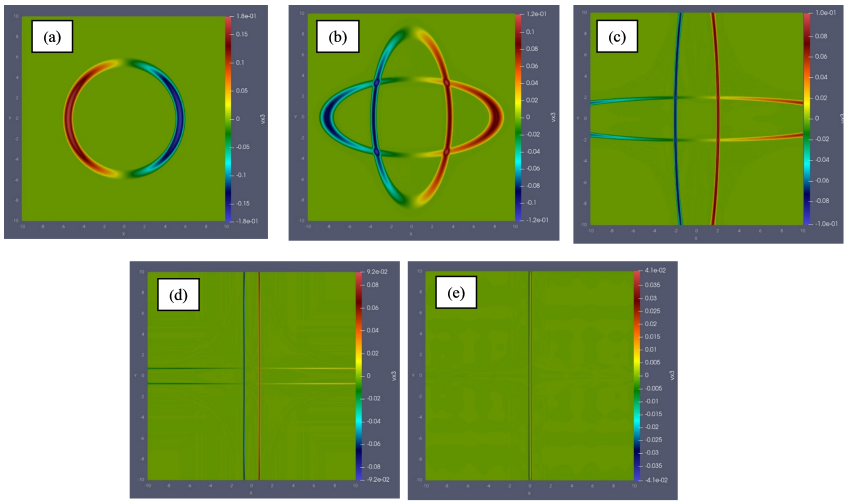

Figure 8: Snapshots of the z-velocity (v_z) in the inwardly propagating rarefaction pulse, for β_0=1and r= $\frac{1}{\sqrt{10}}$ at (a) $t = 0$, (b) $t = 0.4$, (c) $t = 1$, (d) $t = 2$, (e) $t = 4$.

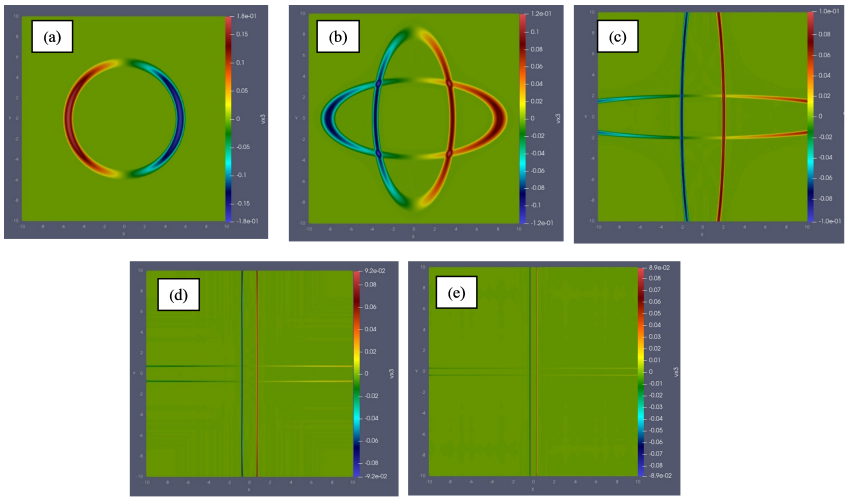

Figure 9: Snapshots of the z velocity (v_z) within the inwardly propagating pulse of rarefaction, for β_0=1 and r= $\frac{1}{10}$ at (a) $t = 0$, (b) $t = 0.4$, (c) $t = 1$, (d) $t = 2$, (e) $t = 4$.

from circular to an elliptical-like form over time. The figures indicate that the changes initiate more promptly as the desired layer approaches the null point. For instance, at time instances $t = 0.4s$, depicted in Figures 2 to 5, the pulse retains its shape at layer r=1, while it undergoes shape alteration at layers r $=\frac{1}{\sqrt{10}}= 0.32$ and r $=\frac{1}{10} = 0.1$.

In accordance with the panels (a) of Figure 14, the red line (β_0= 0, r = 1) shows moderate peaks with a smooth profile. The orange line (β_0 = 1, r = 1) displays higher peaks than the red line, indicating increased radial velocity. The blue dotted line (β_0 = 1, r = 0.32) exhibits sharp, high peaks, suggesting a more complex interaction. The green line (β_0 =

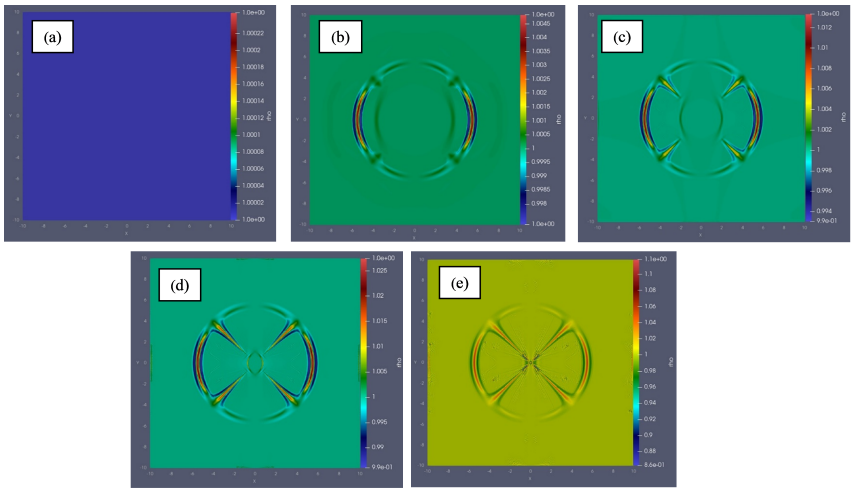

Figure 10: Snapshots of the plasma density in the inward-propagating pulse of rarefaction for β_0=0 and at (a) $t = 0$, (b) $t = 0.4$, (c) $t = 1$, (d) $t = 2$, (e) $t = 4$.

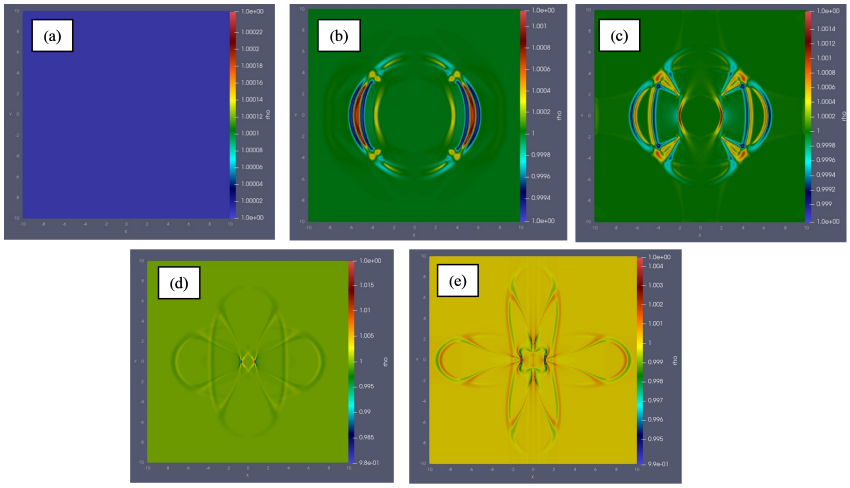

Figure 11: Snapshots of the plasma density in the inward-propagating pulse of rarefaction for β_0=1 at (a) $t = 0$, (b) $t = 0.4$, (c) $t = 1$, (d) $t = 2$, (e) $t = 4$.

1, r = 0.1) shows the lowest amplitude, indicating a decrease in radial velocity. The peaks are well-defined, with noticeable oscillations. The panels (b) of Figure 14 are similar to the panels (a), but the overall amplitude of the curves appears to be slightly lower. The peaks are still present but seem less pronounced compared to the first figure. Here, the oscillations remain evident, but the overall profile is more subdued. In accordance with the panels (c), the peaks are significantly higher than in the previous figures, especially for the orange and blue lines. The red line remains consistent, while the green line shows a slight increase in amplitude. The peaks are sharper and more pronounced, indicating a stronger response at this time. The panels (b) of Figure 14 show a decrease in amplitude for all curves compared

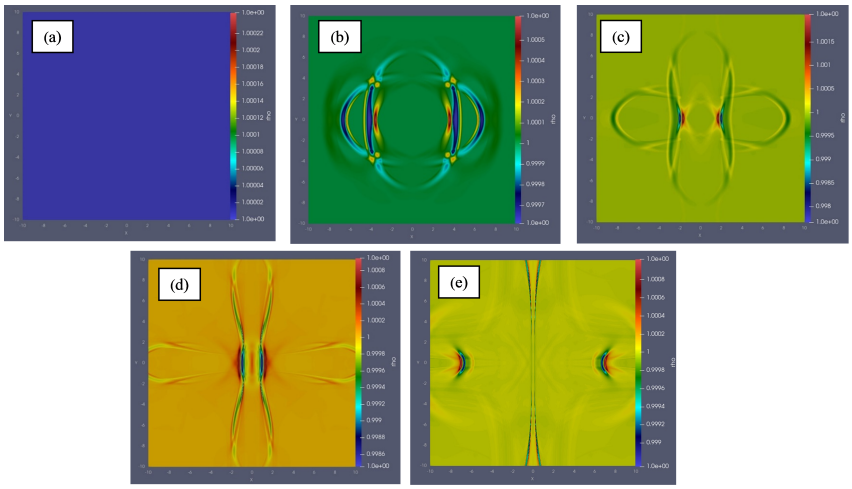

Figure 12: Snapshots of the plasma density in the inward-propagating pulse of rarefaction for β_0=1 at (a) $t = 0$, (b) $t = 0.4$, (c) $t = 1$, (d) $t = 2$, (e) $t = 4$.

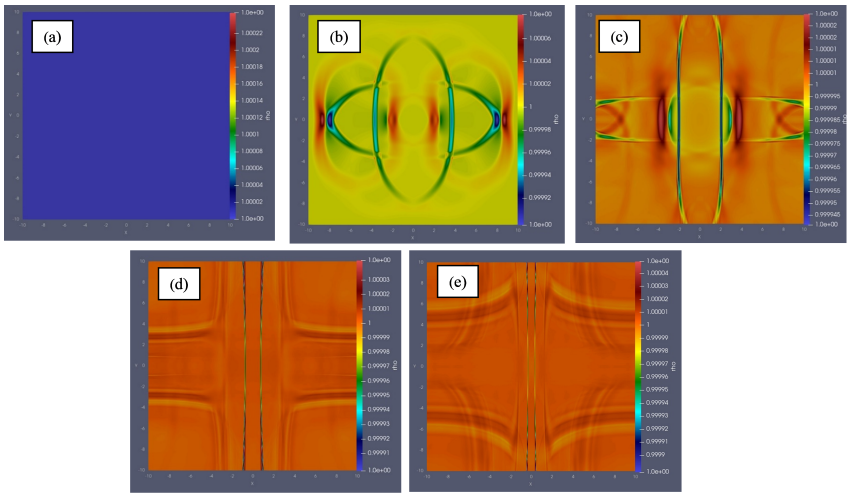

Figure 13: Snapshots of the plasma density in the inward-propagating pulse of rarefaction for β_0=100 at (a) $t = 0$, (b) $t = 0.4$, (c) $t = 1$, (d) $t = 2$, (e) $t = 4$.

to the first figure, while the third figure shows an increase, particularly for the orange and blue lines. The panels (b) of Figure 14 display well-defined peaks, while in the panels (b) of Figure 14, the peaks are slightly rounded. The panels (c) of Figure 14 exhibit sharper peaks, indicating a more dynamic response. The behavior of the curves in Figure 14 suggests that as time progresses, the system's response varies, with some instances showing higher amplitudes and sharper peaks, indicating a more intense interaction of the Alfvén pulse. The variations in amplitude and peak sharpness highlight the dynamic nature of the system, with certain moments exhibiting stronger responses than others. This analysis underscores the sensitivity of the system to the parameters β_0 and r as time evolves. Notably, the closer a

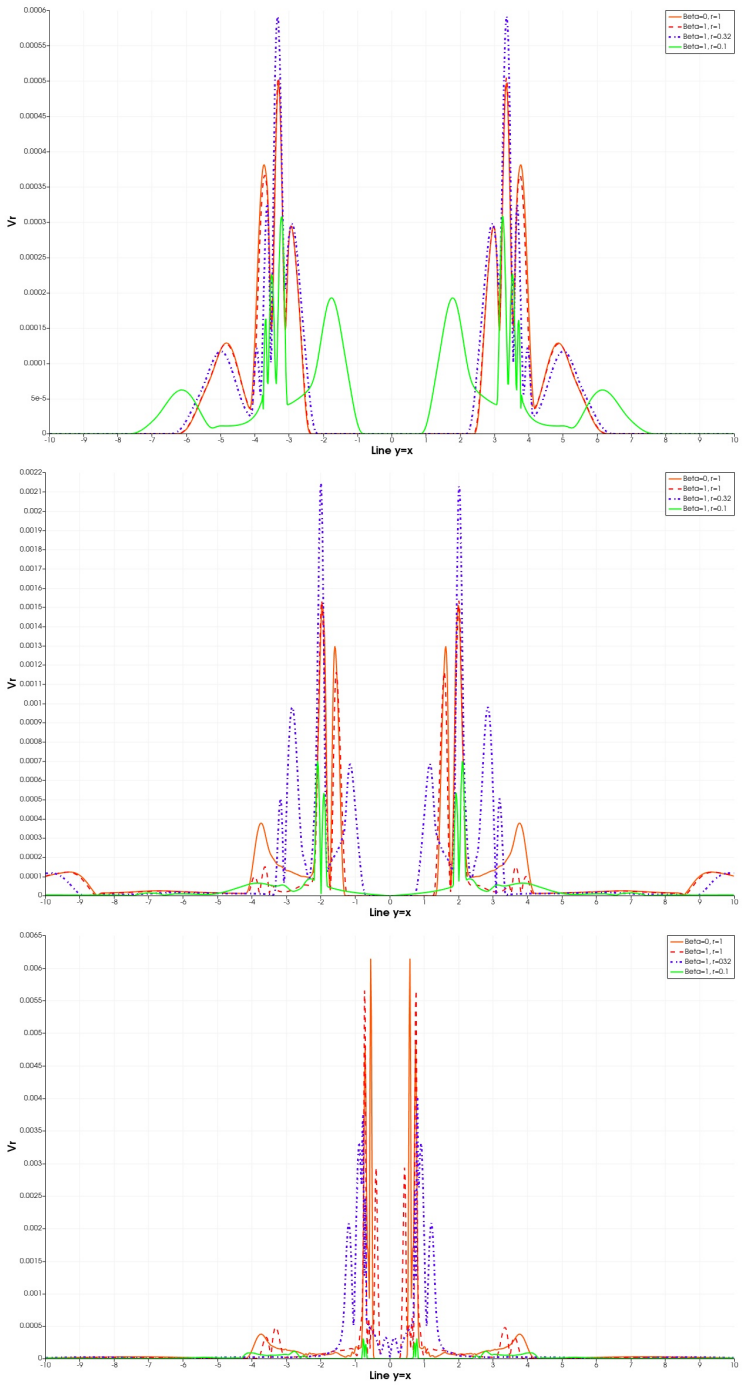

Figure 14: The comparison of radial velocity in the inwardly propagating pulse of rarefaction, $v_r = \sqrt{v_x^2 + v_y^2}$ over line $y = x$ for β_0=0 and r=1, β_0=1 and r=1, β_0=1 and r $=\frac{1}{\sqrt{10}} = 0.32$, and β_0=1 and r $= \frac{1}{10} = 0.1$ at (a) $t = 0.4$, (b) $t = 2$, and (c) $t = 4$.

layer is to the null point, the more pronounced the changes become. Indeed, as we adjust the plasma beta closer to the zero point, the disturbances in radial velocity become smaller, and over time, the wave energy is discharged more rapidly along the field lines.

In accordance with the panels (a) of Figure 15, the red line ($\beta 0 = 0$, r = 1) shows moderate peaks with a smooth profile. The orange line ($\beta_0 = 1$, r = 1) displays higher peaks than the red line, indicating increased density. The blue dotted line ($\beta 0 = 1$, r = 0.32) exhibits sharp peaks, suggesting a more complex interaction. The green line ($\beta_0 = 1$, r = 0.1) shows the lowest amplitude, indicating a decrease in density. The peaks are well-defined, with noticeable oscillations. In accordance with the panels (b) of Figure 15, the overall shape remains similar to the panels (a), but the peaks appear to be slightly lower in amplitude. The red and orange lines maintain their relative heights, while the blue and green lines show less pronounced oscillations. The oscillations are still evident, but the overall profile is more subdued compared to the first figure. In accordance with the panels (c), the peaks are significantly higher than in the previous figures, especially for the orange line. The red line remains consistent, while the blue and green lines show a slight increase in amplitude. The peaks are sharper and more pronounced, indicating a stronger response at this time. The panels (b) show a decrease in amplitude for all curves compared to the panels (a), while the panels (c) show an increase, particularly for the orange line. The panels (a) have well-defined peaks, while the peaks in panels (b) are slightly rounded. The panels (c) exhibit sharper peaks, indicating a more dynamic response. As time progresses from the panels (a) to the panels (c), the system's response varies, sometimes showing higher amplitudes and sharper peaks, indicating a more intense interaction of the rarefaction pulse. The variations in amplitude and peak sharpness highlight the dynamic nature of the system, with certain times exhibiting stronger responses than others. This analysis underscores the system's sensitivity to the parameters β_0 and r as time evolves.

This study reveals significant insights into the interaction of Alfven pulses with a 2D magnetic null point and its implications for solar corona heating. By applying the Pluto code to solve the magnetohydrodynamic equations, we observed that varying the plasma beta parameter profoundly affects the dynamics of the system. The results demonstrate that the Alfven wave exhibits a refraction effect, guiding it toward the null point where it wraps around. Specifically, as the plasma beta β_0 is set to zero, we noted an increase in the magnitude of radial velocity disturbances. This suggests that the energy associated with the Alfven pulses is discharged more efficiently along the magnetic field lines over time, indicating a potential mechanism for energy transfer in the corona. Conversely, when the plasma beta β_0 is set to one near the null point, the density changes exhibited a reduction, implying that the energy transfer dynamics are less effective under these conditions. In contrast, setting the plasma beta to zero resulted in an increase in density changes, highlighting a complex relationship between plasma conditions and the behavior of Alfven waves. Overall, our findings emphasize that both density and velocity changes are intricately linked to the plasma beta and its proximity to the magnetic null point. These results underscore the importance of considering varying atmospheric conditions when assessing energy transfer mechanisms in the solar corona, providing a clearer understanding of the processes that may contribute to its heating and furthering the discourse on wave theory and reconnection theory.

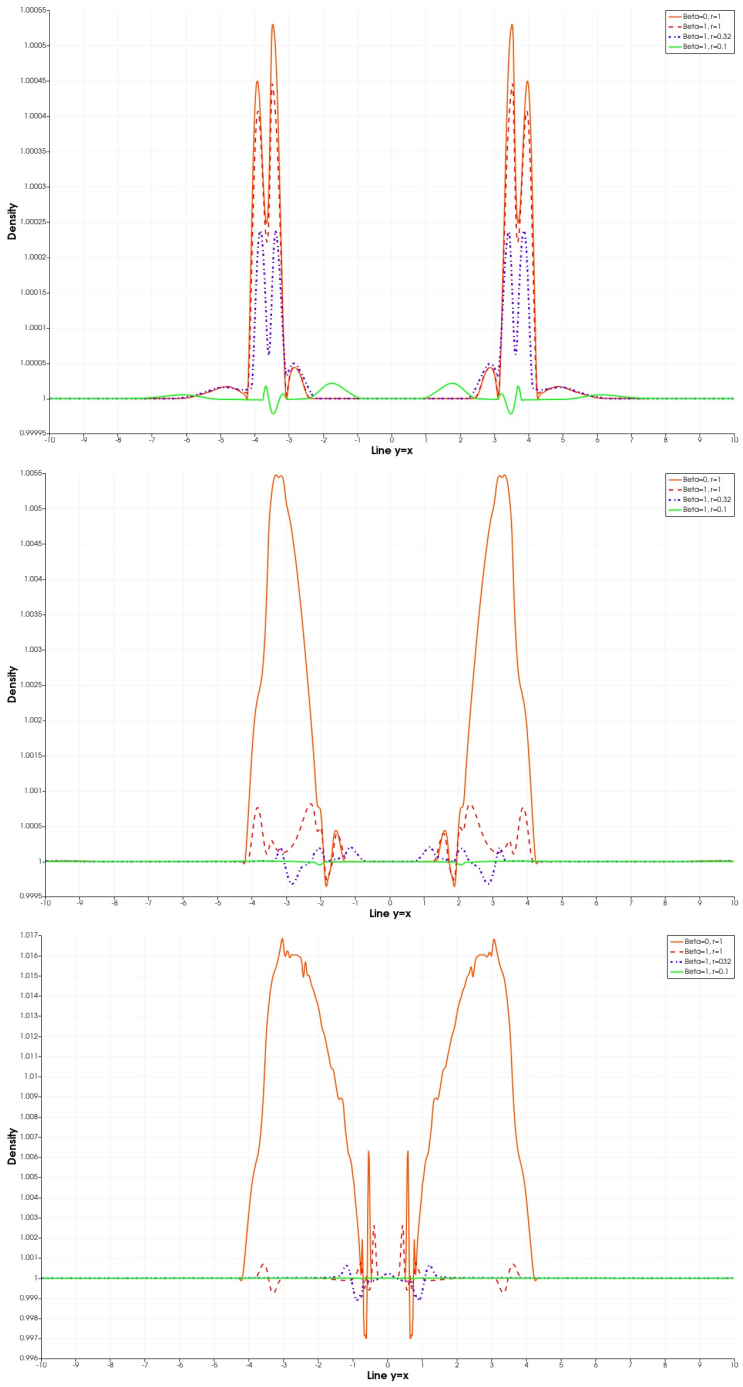

Figure 15: The comparison of plasma density for β_0=0 and r=1, β_0=1 and r=1, β_0=1 and r $=\frac{1}{\sqrt{10}}=0.32$, and β_0=1 and r $=\frac{1}{10}=0.1$ at (a) $t=0.4$, (b) $t=2$, and (c) $t=4$. Over line $y=x$

5 Conclusions

In conclusion, this study offers valuable insights into the mechanisms behind solar corona heating, particularly through the interaction of Alfvén pulses with a two-dimensional magnetic null point. By investigating the nonlinear effects of plasma beta adjustments, we have shown that the dynamics of the corona are highly sensitive to variations in plasma β and their proximity to magnetic null points. Our findings indicate that as plasma β approaches unity near these null points, the system's response becomes more pronounced, characterized by fluctuations in amplitude and peak sharpness. This suggests that the intensity of the Alfvén pulse interaction can vary significantly over time, highlighting the complex interplay between wave phenomena and magnetic reconnection. Furthermore, the results imply that the release of wave energy along magnetic field lines is expedited when plasma β is adjusted closer to the null point, resulting in reduced changes in radial velocity and density disturbances. This emphasizes the importance of considering local atmospheric conditions when evaluating energy transfer mechanisms in the solar corona. By integrating observations of wave phenomena and magnetic reconnection with our theoretical framework, we contribute to a deeper understanding of the processes that heat the solar corona. Ultimately, our study underscores the necessity for further exploration of the intricate relationships between plasma dynamics, magnetic fields, and wave interactions in the solar atmosphere. Continued research in this domain will enhance our understanding of solar activity and its implications for space weather, thereby advancing our knowledge of the fundamental processes governing the Sun's outer layers.

Acknowledgments

We gratefully acknowledge the support provided by Farhangian University for this research endeavor.

Authors' Contributions

All authors have the same contribution.

Data Availability

The data that support the findings of this study are available from the corresponding author upon reasonable request.

Conflicts of Interest

The authors declare no potential conflicts of interest.

Ethical Considerations

The authors have diligently addressed ethical concerns, such as informed consent, plagiarism, data fabrication, misconduct, falsification, double publication, redundancy, submission, and other related matters.

Funding

This research did not receive any grant from funding agencies in the public, commercial, or nonprofit sectors.

References

[1] Tomczyk, S. et al. 2007, Science, 317, 1192.

[2] Zaitsev, V., & Stepanov, A. 1975, A&A, 45, 135.

[3] Edwin, P., & Roberts, B. 1983, Sol. Phys., 88, 179.

[4] Aschwanden, M. J., Fletcher, L., Schrijver, C. J., & Alexander, D. 1999, ApJ, 520, 880.

[5] Nakariakov, V., Ofman, L., Deluca, E., Roberts, B., & Davila, J. 1999, Science, 285, 862.

[6] Sadeghi, R., & Tavabi, E. 2022, MNRAS, 512, 4164.

[7] Tavabi, E., Koutchmy, S., & Ajabshirizadeh, A. 2011, Advances in Space Research, 47, 2019.

[8] Zeighami, S., Tavabi, E., & Amirkhanlou, E. 2020, A&A, 41.

[9] Sadeghi, R., & Tavabi, E. 2024, Advances in Space Research, 74, 3448.

[10] Tavabi, E., & Mollatayefeh, A. 2023, IJAA, 10, 123.

[11] Moreno-Insertis, F., Galsgaard, K., & Ugarte-Urra, I. 2008, ApJ, 673, L211.

[12] Shibata, K. et al. 2007, Science, 318, 1591.

[13] Cirtain, J. et al. 2007, Science, 318, 1580,.

[14] Craig, I. J., & McClymont, A. 1991, University of Waikato Research.

[15] Craig, I. J., & Watson, P. 1992, University of Waikato Research.

[16] 16 Longcope, D,. & Priest, E. 2007, Physics of Plasmas, 14.

[17] McLaughlin, J., & Hood, A. W. 2004, A&A, 420, 1129.

[18] McLaughlin, J., Hood, A. W., & De Moortel, I. 2011, Space Sci. Rev., 158, 205.

[19] Sabri, S., Vasheghani Farahani, S., Ebadi, H., Hosseinpour, M., & Fazel, Z. 2018, MNRAS, 479, 4991.

[20] Sabri, S., Farahani, S. V., Ebadi, H., & Poedts, S. 2020, Scientific Reports, 10, 15603.

[21] Farahani, S. V., & Hejazi, S. 2017, ApJ, 844, 148.

[22] Galsgaard, K., Priest, E., & Titov, V. 2003, J. Geophysical Research: Space Physics, 108.

[23] Thurgood, J., & McLaughlin, J. 2013, A&A, 555, A86.

[24] McLaughlin, J. & Hood, A. W. 2006, A&A, 452, 603.

[25] McLaughlin, J. A., De Moortel, I., Hood, A. W., & Brady, C. S. 2009, A&A, 493, 227.

[26] Brown, D., & Priest, E. R. 2001, A&A, 367, 339.

[27] Gruszecki, M., Farahani, S. V., Nakariakov, V. M., & Arber, T. 2011, A&A, 531, A63.

[28] McLaughlin, J., & Hood, A. W. 2005, A&A, 435, 313.

[29] Zaqarashvili, T. V., & Murawski, K. J. A. 2007, A&A, 470, 353.

[30] Vasheghani Farahani, S., Nakariakov, V. M., & Van Doorsselaere, T. J. A. 2010, A&A, 517, A29.

[31] Vasheghani Farahani, S., Nakariakov, V. M., Verwichte, E., & Van Doorsselaere, T. J. A. 2012, A&A, 544, A127.

[32] Tikhonchuk, V. T., Rankin, R., Frycz, P., & Samson, J. C. 1995, Physics of Plasmas, 2, 501.

[33] Nakariakov, V. M., Mendoza-Briceño, C. A., & Ibáñez S, M. 2000, ApJ, 528, 767.

[34] Suzuki, T. K. 2011, Space Sci. Rev., 158, 339.

[35] Vasheghani Farahani, S., Nakariakov, V. M., Van Doorsselaere, T., & Verwichte, E. J. A. 2011, 39th COSPAR Scientific Assembly, 526, A80.

[36] McLaughlin, J. A., & Hood, A. W. J. A. 2004, A&A, 420, 1129.

[37] Murawski, K., & Roberts, B. 1993, Sol. Phys., 144, 255.

[38] McLaughlin, J. A., Hood, A. W., & de Moortel, I. 2011, Space Sci. Rev., 158, 205.

[39] Thurgood, J. O., & McLaughlin, J. A. J. A. 2013, A&A, 558, A127.

[40] Mignone, A. et al. 2007, ApJS, 170, 228.

[41] Mignone, A. et al. 2023, ApJS, 198, 7.

[42] Karampelas, K., McLaughlin, J. A., Botha, G. J., & Régnier, S. 2023, ApJ, 943, 131.

[43] Sabri, S., Vasheghani Farahani, S., Ebadi, H., Hosseinpour, M., & Fazel, Z. 2018, MNRAS, 479, 4991.

[44] McLaughlin, J. A., De Moortel, I., Hood, A. W., & Brady, C. S. J. A. 2009, A&A, 493, 227.